Available online at www.sciencedirect.com
SCIENCE DIRECT
Thermochimica Acta 432 (2005) 2–9
thermochimica acta
www.elsevier.com/locate/tca

Isothermal and non-isothermal kinetic study of the $PbGeO_3$ solid–solid phase transition

C. Tomasi [a,*], M. Scavini [b], A. Cavicchioli [b], A. Speghini [c], M. Bettinelli [c]

[a] *I.E.N.I.-C.N.R. sez. di Pavia and Dipartimento di Chimica Fisica, Università di Pavia, Viale Taramelli 16, I-27100 Pavia, Italy*
[b] *Dipartimento di Chimica Fisica ed Elettrochimica, Università di Milano, Via Golgi 19, I-20133 Milano, Italy*
[c] *Dipartimento Scientifico e Tecnologico, Università di Verona, and INSTM, UdR Verona, Ca' Vignal, Strada Le Grazie 15, I-37134 Verona, Italy*

Received 21 June 2004; received in revised form 7 February 2005; accepted 19 February 2005

Abstract

A kinetics study on $PbGeO_3$ solid–solid phase transition was realised by means of differential scanning calorimetry and time-resolved X-ray powder diffraction. Isothermal and non-isothermal Johnson–Mehl–Avrami equations were applied to obtain both the activation energy E_a and the Avrami coefficient *n*. The latter parameter has been related to morphological evidences collected by scanning electron microscopy. The limits of the applied theory, i.e., the Arrhenian behaviour of the growth rate and a steady-state nucleation rate, are finally discussed in terms of recent theoretical developments.

Keywords: Germanates; Solid–solid phase transition; Avrami coefficient; Time-solved XRPD

1. Introduction

$x\mathrm{PbO}(1-x)\mathrm{GeO_2}$ glasses received attention because of their promising optical applications when doped with rare earths [1,2]. Both the glass forming region and the phase equilibria of the $x\mathrm{PbO}(1-x)\mathrm{GeO_2}$ system have been recently investigated by our group in the $0.00 \leq x \leq 0.50$ range. In such a compositional range, homogeneous glass is obtained only for $x > 0.25$ because of the segregation of nanocrystalline GeO_2 for lower Pb content [3]. The phase equilibria study starting from glassy materials resulted difficult since the devitrification process led to the formation of several metastable phases [4]. For instance, devitrification of the $x = 0.50$ glass produced monoclinic lead metagermanate $PbGeO_3$ [5] via the formation of a metastable phase, unknown in literature.

An isothermal and non-isothermal kinetic study on the formation of the metastable phase from devitrification of glassy lead metagermanate was lately reported by our group [6]. Besides an activation energy value of about 320 kJ mol^{-1}, that is reasonably consistent with the devitrification of a number of oxide glasses, an Avrami coefficient $n \approx 1.3$ was found. An attempt to relate such a coefficient to morphological evidence from secondary electron imagery collected by scanning electron microscopy (SEM) did not give encouraging results.

A non-integer Avrami coefficient for the devitrification of $Se_{0.7}Ge_{0.2}Sb_{0.1}$ glasses was also reported by Afify et al. [7], who accounted for the value of $n = 1.5$ as an overlapping of two mechanisms with $n = 1$ and $n = 2$. Even in the case of glassy $PbGeO_3$, recent preliminary measurements point to a similar interpretation. In fact, X-ray diffraction patterns collected on samples heat-treated at a temperature just above the crystallisation peak highlighted the presence of both the unknown and the monoclinic $PbGeO_3$ phases.

The present paper focused on the kinetics of the solid–solid transition between the metastable and the monoclinic $PbGeO_3$ phases. The activation energy (E_a) and the Avrami coefficient (n) were determined by both isothermal and non-isothermal methods by differential scanning

* Corresponding author.
E-mail address: corrado.tomasi@unipv.it (C. Tomasi).

0040-6031/$ – see front matter © 2005 Elsevier B.V. All rights reserved.
doi:10.1016/j.tca.2005.02.036

calorimetry (DSC) and time-resolved X-ray powder diffraction (XRPD).

As reported in our previous paper [6], several mathematical approaches regarding the DSC and TGA data analysis of non-isothermal reaction kinetics are accessible in literature. Although based on the same formal theory, great differences in assumptions can lead to incongruous results [8–11].

2. Experimental

2.1. Sample preparation

Pure metastable $PbGeO_3$ cannot be produced by devitrification of glassy lead metagermanate. Therefore, single crystals of the metastable phase were produced by mixing stoichiometric amounts of PbO (>99.9%) and GeO_2 (99.998%), and thermally treating the mixture in an electric furnace according to the following procedure: (I) heating to 1100 °C at 250 °C/h; (II) holding this temperature for 1 h; (III) cooling down to 700 °C at 100 °C/h; (IV) cooling down to room temperature by switching off the furnace.

2.2. Measurements

DSC measurements were performed in a 2910 DSC (TA Instruments), fitted with a standard DSC cell. Powdered samples (∼50 mg) were introduced in silver pans, and run at 1, 2, 5, 10, 15, and 20 °C/min, between 500 and 650 °C, under nitrogen purge. Isothermal data were collected at temperatures ranging between 555 °C and 570 °C, on similar amounts of powders under nitrogen.

Secondary electron imagery of fractured surface was obtained with a JEOL JXA 840A scanning electron microscope at an accelerating voltage of 20 kV.

Temperature scanning XRPD experiments were done on the GILDA beamline at the European Synchrotron Radiation Facility (ESRF, Grenoble, France) with a Debye–Scherrer experimental geometry. Samples were put in quartz capillaries (Ø = 0.3 mm), which, in turn, were mounted on a rotating system. The wavelength was 0.688043 Å. All diffraction patterns were collected by an image plate (IP, *Fuji* 200 mm × 400 mm) with a sample to detector distance of 274.12 mm. For a complete description of the experimental apparatus, see [12]. XRPD experiments were done at 1 °C/min between 400 and 700 °C. Temperature resolved data were collected by the so-called "translating imaging plate technique" [13]. Data integration was done using scan-t13 program. Each IP was divided in stripes corresponding to $\Delta T \sim 3.3$ K. Experiments were repeated twice to determine reproducibility.

3. Theoretical aspects

The theory of kinetics used to interpret the DTA and DSC measurements was proposed by Johnson and Mehl [14], and Avrami [15–17], similarly developed by Kolomogoroff [18] and later by Erofeev and Mitzkevich [19]. The basic form describes the evolution of the volume transformed fraction α as a function of time *t:*

$$\alpha = 1 - \exp\left[-g\int_0^t I_v\left(\int_{t'}^t u\,d\tau\right)^m dt'\right] \quad (1)$$

where g is a geometric factor, I_v the nucleation frequency per unit volume, u the crystal growth rate and m is a dimensionless exponent related to the morphology of the crystal growth. It is commonly accepted that, according to the mechanisms of growth, the exponent m can be an integer or a half integer: (I) for interface-controlled growth it assumes the values of 1, 2, 3 for one-, two-, and three-dimensional growth, respectively, (II) for diffusion-controlled growth where u decreases with $t^{-1/2}$, it assumes the values of 1/2, 1, 3/2 for the respective dimensionalities of growth [15–17].

Crystallisation and reaction kinetics at a constant temperature are generally expressed by the well known Johnson–Mehl–Avrami (JMA) equation:

$$-\ln(1-\alpha) = (kt)^n \quad (2)$$

where $n = m + 1$ and k is the rate constant which includes nucleation and growth. Within a narrow temperature range, the temperature dependence of k is considered to be described by the Arrhenius equation:

$$k = \nu \exp\left(-\frac{E_a}{RT}\right) \quad (3)$$

where E_a and ν are the activation energy and the frequency factor for the overall process, R the universal gas constant and T is the absolute temperature. The logarithmic form of Eq. (2):

$$\ln[-\ln(1-\alpha)] = n\ \ln k + n\ \ln t \quad (4)$$

allows evaluation of both n and k from isothermal measurements as the slope and intercept of the $\ln[-\ln(1-\alpha)]$ versus $\ln t$ plot. E_a may also be assessed from the logarithmic form of Eq. (3):

$$\ln k = \ln \nu - \frac{E_a}{RT} \quad (5)$$

from the slope of the $\ln k$ versus $1/T$ plot.

On DSC and DTA experiments the heating rate $\beta = (dT/dt)$ is usually kept constant during the whole scan. Thus, the rate constant k changes with time as the temperature changes. Among the various expressions derived from Eq. (1) describing non-isothermal kinetics, some lead to activation energy values in good agreement with those obtained by isothermal experiments [8]. The non-isothermal methods employed in the present paper are summarised in the following.

3.1. The Ozawa method

With no additive assumption, the Ozawa method [20] provides the Avrami coefficient n straightforwardly from the

JMA equation, by taking into account a constant heating rate.

$$\left.\frac{\mathrm{d}\{\log[-\ln(1-\alpha)]\}}{\mathrm{d}\log\beta}\right|_T = -n \tag{6}$$

Thus, by recording DSC runs at different heating rates, at given temperatures the $\log[-\ln(1-\alpha)]$ versus $\log\beta$ should be linear with slope $-n$.

3.2. The Ozawa–Chen method

This method [21,22] is used to evaluate the activation energy of the process by supposing that, at the peak maximum, the transformed fraction α' is constant. Hence, given a set of DSC runs at various scan rates, E_a can be obtained from the expression:

$$\left.\frac{\mathrm{d}\ln(T'^2/\beta)}{\mathrm{d}(1/T')}\right|_{\alpha'} = \frac{E_a}{R} \tag{7}$$

by plotting $\ln(T'^2/\beta)$ versus $1/T$ at a given α'.

3.3. The Takhor method

The Takhor method [23] represents an alternative method for the estimation of E_a. By assuming that the maximum transformation rate is achieved at the peak maximum T_p, the activation energy can be obtained by the slope of $\ln\beta$ versus $1/T_p$ plot, i.e.:

$$\frac{\mathrm{d}\ln\beta}{\mathrm{d}(1/T_p)} = -\frac{E_a}{R} \tag{8}$$

This method is based on the incorrect assumption of ignoring the time dependence of the rate constant k.

3.4. The Kissinger method

Although based on a different approach, this method [24] leads to results similar to those obtained by Ozawa and Chen. By introducing some simplifications, Kissinger showed that for any transformation, the $\ln(\beta/T_p^2)$ versus $1/T_p$ plot is linear with slope E_a/R.

3.5. The Coats–Redfern–Sestak method

Coats and Redfern [25], and later Sestak [26], described a reliable method to determine the activation energy of transformations. By considering the reaction rate in the form:

$$\left(\frac{\mathrm{d}\alpha}{\mathrm{d}t}\right) = g(\alpha)h(T) \tag{9}$$

They identified $h(T)$ as the rate constant k. Suitable substitutions and integrations yield the expression:

$$\left|\frac{1}{n}\ln[-\ln(1-\alpha')] - 2\ln T' = \ln\frac{K_0 R}{nE_a\beta} - \frac{E_a}{RT'}\right. \tag{10}$$

where K_0 and β are constants.

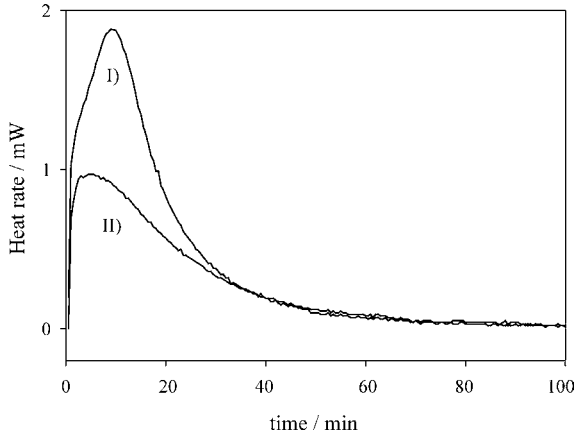

Fig. 1. DSC isothermal profile at 570 °C performed on $PbGeO_3$ metastable single crystals. Signal recorded on a fresh specimen (curve I); second record on the just transformed sample (curve II).

Hence, when the value of the Avrami exponent n is known, the activation energy E_a can be obtained from the slope of the $n^{-1}\ln[-\ln(1-\alpha')] - 2\ln T'$ versus $1/T'$ plot.

4. Results

4.1. Isothermal measurements

Isothermal measurements on metastable $PbGeO_3$ single crystals were performed between 555 and 570 °C for different lengths of time until a horizontal line was achieved. The trace recorded at 570 °C is reported in curve I of Fig. 1. The instrumental drift correction was obtained by subtracting the trace for the transformed sample (curve II) from the original signal (curve I).

At a given time t, the transformed fraction α is determined by the ratio between the area under the exotherm up to time t and the total peak area. Fig. 2 gives α as a function of time at $T = 555$, 560, 565 and 570 °C. These temperatures were chosen to complete the transformation in a minimum of 30 min, reducing the effect of the initial time uncertainty. Avrami plots of the isothermal data are given in Fig. 3. The plots are approximately linear and parallel with slope n (see Table 1). The activation energy is assessed by the slope of the Arrhenius plot shown in Fig. 4.

4.2. Non-isothermal DSC measurements

The DSC traces recorded at different heating rates on $PbGeO_3$ metastable single crystals are reported in Fig. 5. For each curve, only the solid–solid phase transition region is shown. To make a better comparison, the heat rate has been normalised to the heating rate. As expected, the peak temperature increases as the heating rate increases.

According to Ozawa, in Fig. 6 $\log[-\ln(1-\alpha)]$ is plotted versus the logarithm of the heating rate, and the Avrami coefficient n is estimated from the slope of the lines.

Table 1
Kinetic parameters from isothermal and non-isothermal methods

Method	Technique	Activation energy, E_a (kJ/mol)	Avrami coefficient, n
Isothermal	DSC	419 ± 55	2.41 ± 0.23
Ozawa	DSC		2.56 ± 0.18
Ozawa–Chen/Kissinger	DSC	370 ± 11	
Takhor	DSC	386 ± 20	
Coats–Redfern–Sestak (γ_{meta})	XRPD	392 ± 10	from Ozawa
Coats–Redfern–Sestak (γ_{stab})	XRPD	360 ± 37	from Ozawa

Following Ozawa and Chen, and Kissinger methods, Fig. 7 shows the logarithmic plot of (T'^2/β) as a function of $1/T$ for different values of α. The fitted linear plots have slope E_a/R.

The Takhor plot, $\ln \beta$ versus $1/T_p$, is reported in Fig. 8. The data are linear with slope $-E_a/R$.

4.3. XRPD results

Scanning time-resolved XRPD patterns at 1 °C/min shows the $PbGeO_3$ solid–solid phase transition occurring between 558 and 585 °C (Figs. 5 and 9). Patterns collected out of this range show that for $T \leq 558$ °C only peaks relative to the metastable phase are apparent, whilst for $T \geq 585$ °C only the stable phase is detected.

Quantitative analysis was done on the areas of selected XRPD peaks. The Alexander and Klug model [27] was applied assuming the same density for the two $PbGeO_3$ polymorphs. For each temperature, the volume fraction γ of both phases is determined by averaging the I/I_0 ratios, where I is the area of a given peak and I_0 is the area of the same peak in the pure phase. The volume transformed fraction $\alpha = \gamma_{stab} = 1 - \gamma_{meta}$, where γ_{stab} and γ_{meta} are the volume fraction of the stable and metastable phases, respectively, is reported in Fig. 10a as a function of temperature. In Fig. 10b the same data are plotted according to the Coats–Redfern–Sestak method, taking $n = 2.56$ as determined by the Ozawa method. An activation energy E_a equal to 392 ± 9 and 360 ± 37 kJ/mol has been obtained from γ_{meta} and γ_{stab}, respectively (see Table 1).

5. Discussion

The comparison of isothermal and scanning methods shows fairly good agreement for both the activation energy E_a and the Avrami coefficient n of the $PbGeO_3$ solid–solid transition (see Table 1). Such an agreement points out two interesting aspects: (I) the application of the Coats–Redfern–Sestak method to time-resolved diffraction

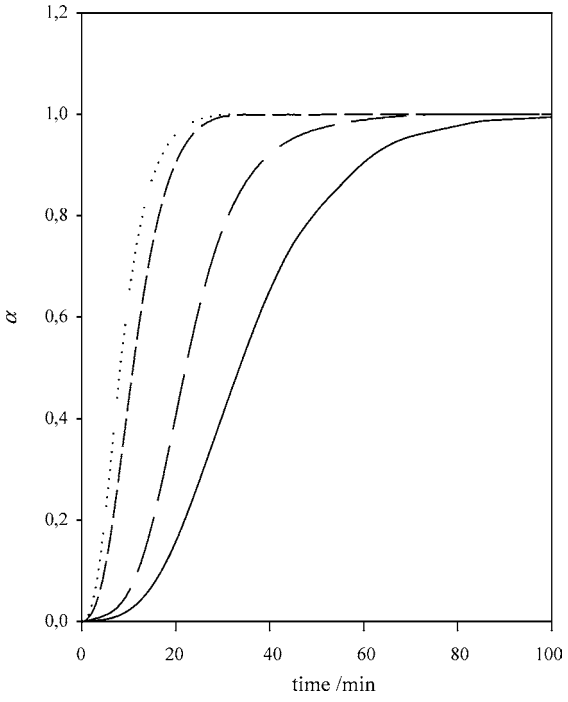

Fig. 2. Volume of the transformed fraction α as a function of time from isothermal measurements at $T = 555$ °C (solid line); $T = 560$ °C (long dash); $T = 565$ °C (short dash); $T = 570$ (dotted).

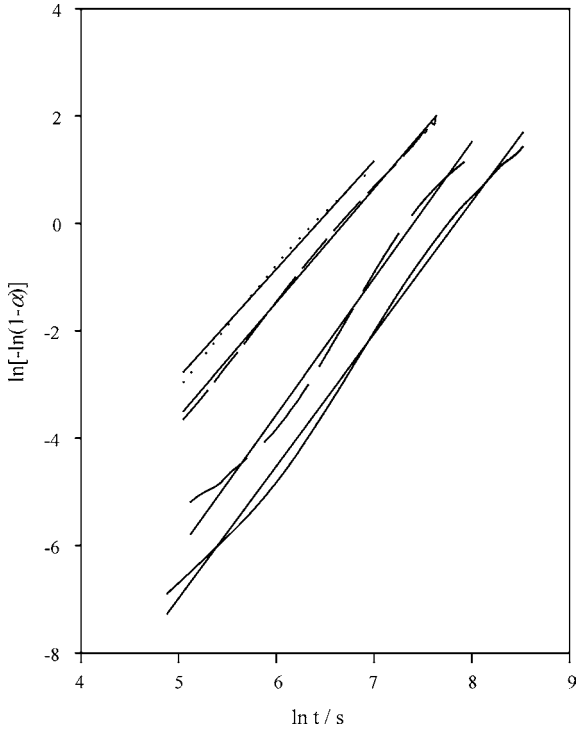

Fig. 3. Avrami plots for isothermal $PbGeO_3$ solid–solid phase transition. $T = 555$ °C (solid line); $T = 560$ °C (long dash); $T = 565$ °C (short dash); $T = 570$ (dotted).

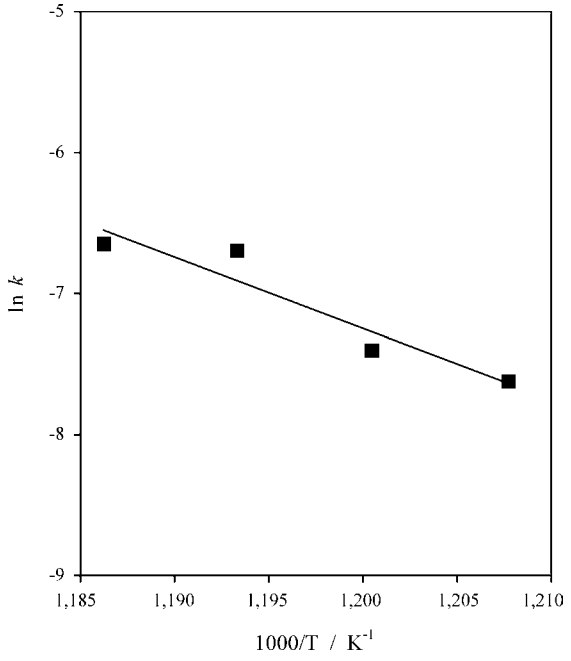

Fig. 4. Arrhenius plot for isothermal $PbGeO_3$ solid–solid phase transition.

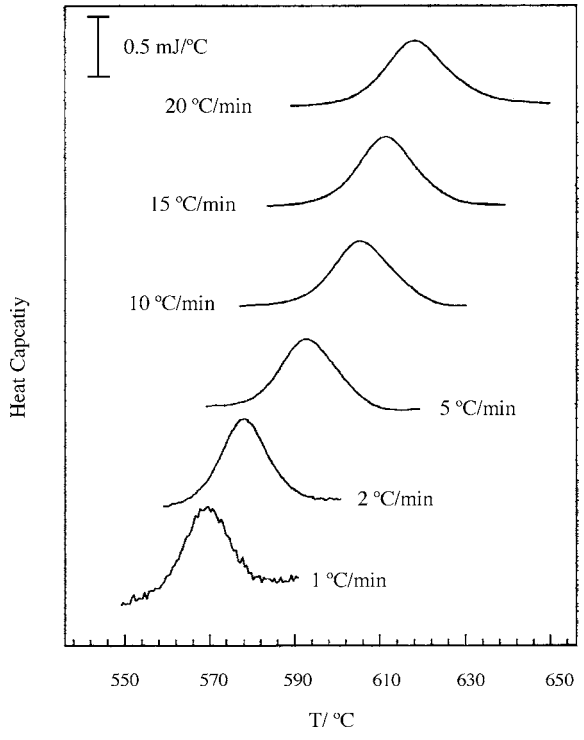

Fig. 5. DSC traces recorded on $PbGeO_3$ metastable single crystals at different heating rates. For the sake of clarity, only the solid–solid phase transition regions are shown.

data, i.e., a "non-classical" thermal method, can be used as an alternative way to estimate E_a; (II) the assumptions made for the extension of the Avrami theory to non-isothermal measurements are acceptable, in the present case. The higher activation energy obtained by the isothermal method than

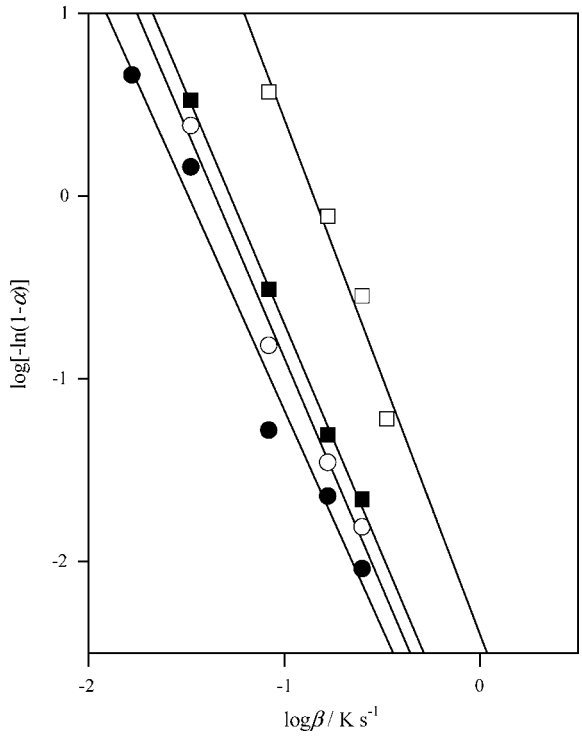

Fig. 6. Ozawa plot for non-isothermal $PbGeO_3$ solid–solid phase transition. $T = 583\,^{\circ}C$ (open squares); $T = 587\,^{\circ}C$ (filled squares); $T = 590\,^{\circ}C$ (open circles); $T = 607\,^{\circ}C$ (filled circles).

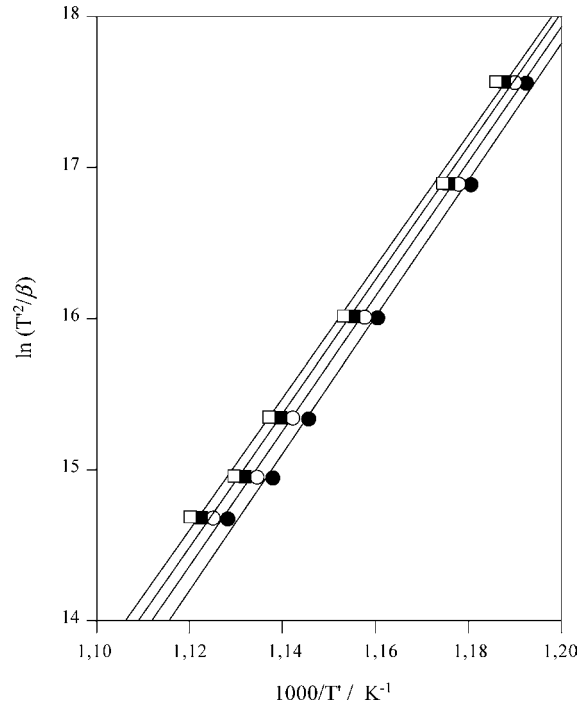

Fig. 7. Ozawa and Chen, and Kissinger plots for non-isothermal $PbGeO_3$ solid–solid phase transition. $\alpha = 0.2$ (filled circles); $\alpha = 0.3$ (open circles); $\alpha = 0.4$ (filled squares); at peak maximum (open squares).

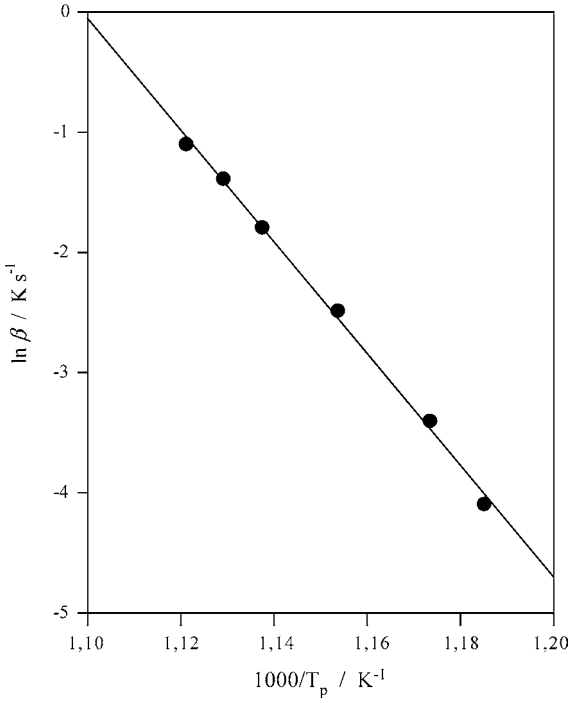

Fig. 8. Takhor plot for non-isothermal $PbGeO_3$ solid–solid phase transition.

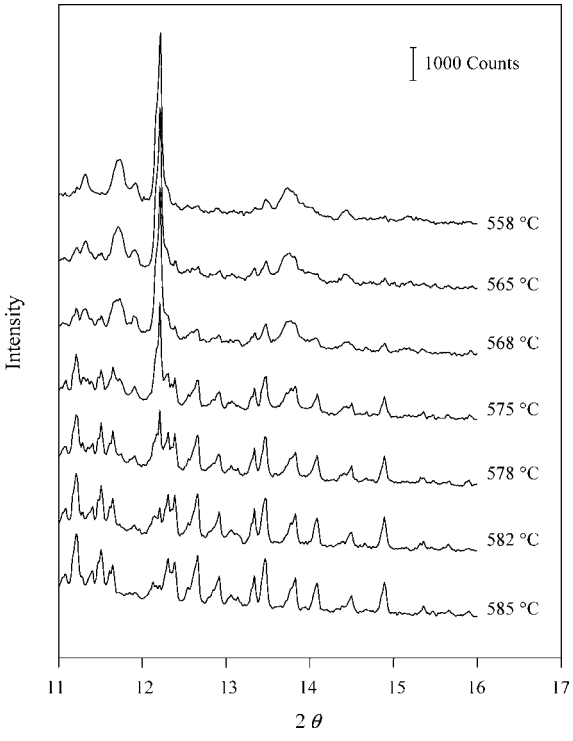

Fig. 9. Non-isothermal time-resolved XRPD patterns in the solid–solid phase transition domain.

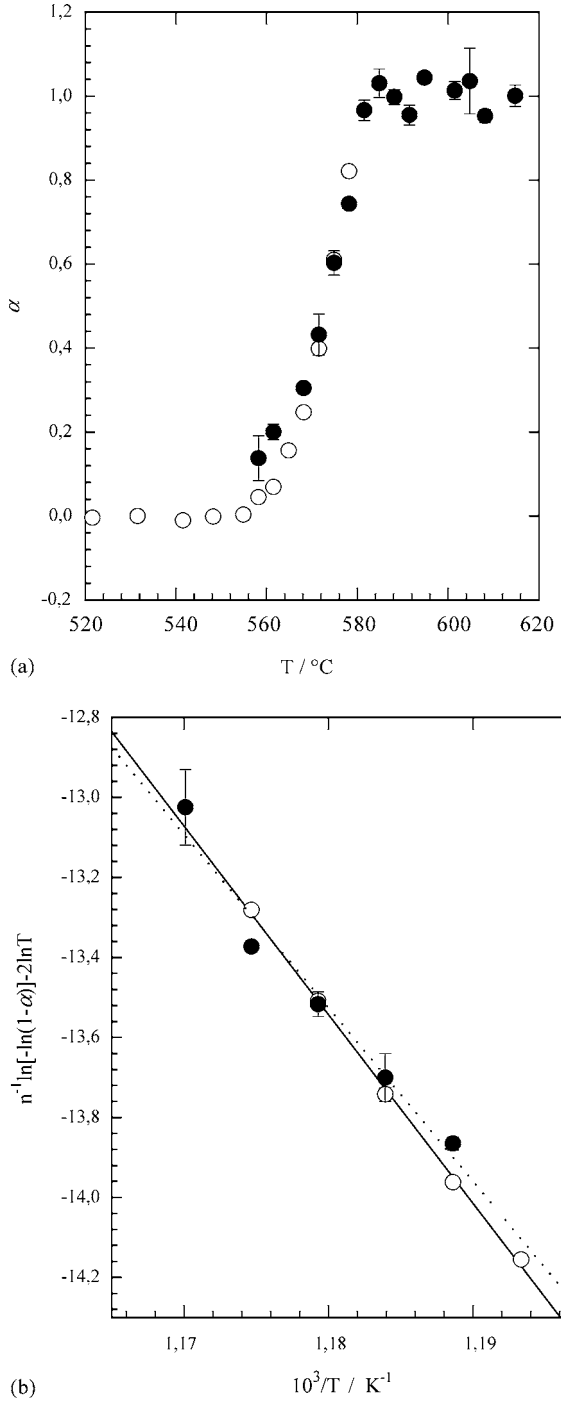

Fig. 10. Volume transformed fraction α evaluated from time-resolved XRPD data: (a) plotted vs. temperature; (b) plotted according to the Coats–Redfern–Sestak method. Metastable phase (open circles); stable phase (filled circles).

the non-isothermal methods is likely due to the large experimental error in the isothermal data caused by the limited number of temperatures (see Table 1). The mean value of ≈385 kJ/mol is consistent with both the value of 323 kJ/mol found by our group for the devitrification of lead metagermate glass [6], and the 233 kJ/mol for the crystallisation of amorphous GeO_2 [28].

Our previous paper [6] discussed the different meanings assigned to the Avrami coefficient n by various authors. If we rely on the common accepted meaning that for interface-controlled growth, $m = n - 1$ should be interpreted as the dimensionality of the crystal growth, our

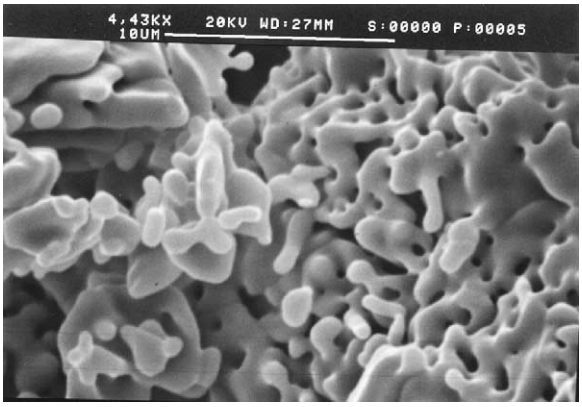

Fig. 11. Secondary electron imagery collected by scanning electron microscope (SEM) on $PbGeO_3$ heat-treated at 590 °C.

experimental data suggest a one-dimensional interface-controlled mechanism. This seems to be consistent with the secondary electron imagery of Fig. 11 where finger shaped crystals are detected on samples heat-treated above the solid–solid transition (590 °C). In present case, in view of the structural evolution of $PbGeO_3$ determined by time-resolved XRPD evidences, the non-integer value of $n \approx 2.5$ ($m = 1.5$) cannot be interpreted as the overlaying of two different mechanisms as suggested by Afify et al. [7].

The assumptions of an Arrhenian behaviour of the growth rate and a steady-state nucleation rate in the JMA theory are sometimes incorrect. A number of recent works are devoted to the applicability of these approximations. Kelton et al. [29] presented a model for simulating polymorphic crystallisation under both isothermal and non-isothermal conditions, including time-dependent nucleation rates and cluster-size dependent growth rates. Their experimental DSC/DTA data on lithium disilicate glasses were in good agreement with calculations taking into account both particle size and shape.

Another analytical approach to DSC/DTA crystallisation data via homogeneous nucleation and growth of crystallites was developed by Shneidman and Uhlmann [30] without involving an Arrhenian dependence of the growth rate. By analysing DTA data on the devitrification of *o*-terphenyl, they showed that the steady-state nucleation assumption is not successful, and, according to further experimental evidences, such a situation seems to be more typical than exceptional. Consequently, the application of a time-dependent nucleation rate led to an "effective Avrami exponent" ≈5, which cannot be related to the crystal morphology. A statistical model able to evaluate microstructure development during nucleation and growth, in the framework of the JMA theory, has lately been proposed by Pineda and Crespo [31]. For a given grain size distribution, the authors estimated an effective growth rate according to the previous grain history.

6. Summary

The kinetics study of the $PbGeO_3$ solid–solid phase transition based on the Johnson–Mehl–Avrami theory has been carried out by means of DSC and time-resolved XRPD measurements. A fairly good agreement between isothermal and non-isothermal data was found. The mean activation energy value of ≈385 kJ/mol is consistent with a number E_a data reported in literature for both glass crystallisation and solid–solid phase transition. The Avrami coefficient n has been successfully related to morphological evidences produced by secondary electron microscopy. The reliability of the present results point out that the assumptions of the Arrhenian behaviour for both the growth and the nucleation rates, are fulfilled.

Acknowledgements

The authors acknowledge the European Synchrotron Radiation Facility for provision of synchrotron radiation facilities; they would also like to thank Dr. Carlo Meneghini for assistance in using beamline BM08 (GILDA-CRG) and Dr. Luca Mollica who collected the XRPD patterns. The authors are finally grateful to Dr. F. Maglia for helping in collecting SEM images.

References

[1] S. Mailis, A.A. Anderson, S.J. Barrington, W.S. Brocklesby, R. Greef, H.N. Rutt, R.W. Eason, Opt. Lett. 23 (1998) 1751.
[2] D. Lezal, J. Pedlíková, J. Horák, J. Non-Cryst. Solids 196 (1996) 178.
[3] P. Ghigna, P. Mustarelli, C. Tomasi, E. Quartarone, M. Scavini, A. Speghini, M. Bettinelli, J. Phys. Chem. B 106 (2002) 9802.
[4] M. Scavini, C. Tomasi, A. Speghini, M. Bettinelli, J. Mat. Synth. Process. 9 (2001) 93.
[5] Y.Z. Nozik, B.A. Maksimov, L.E. Fykin, V.Ya. Dudarev, L.S. Garashina, V.T. Gabrielyan, Zh. Strukt. Khim. 19 (1978) 731.
[6] C. Tomasi, M. Scavini, A. Speghini, M. Bettinelli, M.P. Riccardi, J. Therm. Anal. Calorim. 70 (2002) 151.
[7] N. Afify, M.A. Abdel-Rahim, A.S. Abd El-Halim, M.M. Hafiz, J. Non-Cryst. Solids 128 (1991) 269.
[8] H. Yinnon, D.R. Uhlmann, J. Non-Cryst. Solids 54 (1983) 253.
[9] D.W. Henderson, J. Non-Cryst. Solids 30 (1979) 301.
[10] T.J.W. De Bruijn, W.A. De Jong, P.J. Van der Berg, Thermochim. Acta 45 (1981) 315.
[11] J.M. Criado, A. Ortega, J. Therm. Anal. 29 (1984) 1075.
[12] C. Meneghini, G. Artioli, A. Balerna, A.F. Gualtieri, P. Norby, S. Mobilio, J. Synchrotron. Rad. 8 (2001) 1162.
[13] P. Norby, J. Appl. Cryst. 30 (1997) 21.
[14] W.A. Johnson, K.F. Mehl, Trans. Am. Inst. Min. Met. Eng. 135 (1939) 419.
[15] M. Avrami, J. Chem. Phys. 7 (1939) 1103.
[16] M. Avrami, J. Chem. Phys. 8 (1940) 212.
[17] M. Avrami, J. Chem. Phys. 9 (1941) 177.
[18] A.N. Kolomogoroff, Izvestiya Akad. Nauk USSR Ser. Math. 1 (1937) 355.
[19] B.V. Erofeev, N.I. Mitzkevich, Reactivity of Solids, Elsevier, Amsterdam, 1956, p. 225.

[20] T. Ozawa, Polymer 12 (1971) 150.
[21] T. Ozawa, Bull. Chem. Soc. Jpn. 38 (1965) 1881.
[22] H.S. Chen, J. Non-Cryst. Solids 27 (1978) 257.
[23] R.L. Takhor, Advances in Nucleation and Crystallization of Glasses, American Ceramic Society, Columbus, 1972, p. 166.
[24] H.E. Kissinger, J. Res. NBS 57 (1956) 217.
[25] A.W. Coats, J.P. Redfern, Nature 201 (1964) 68.
[26] J. Sestak, Phys. Chem. Glasses 15 (1974) 137.
[27] L. Alexander, H.P. Klug, Basic aspect of X-ray absorption in quantitative diffraction analysis of powder mixtures, Anal. Chem. 20 (10) (1948).
[28] A. Montenero, E. Baiocchi, M. Bettinelli, L. Di Sipio, A. Sotgiu, Mat. Chem. Phys. 8 (1983) 379.
[29] K.F. Kelton, K. Lakshmi Narayan, L.E. Levine, T.C. Cull, C.S. Ray, J. Non-Cryst. Solids 204 (1996) 13.
[30] V.A. Shneidman, D.R. Uhlmann, J. Chem. Phys. 109 (1998) 186.
[31] E. Pineda, D. Crespo, Phys. Rew. B 60 (1999) 3104.